Algal Research 85 (2025) 103889

Contents lists available at ScienceDirect

Algal Research

journal homepage: www.elsevier.com/locate/algal

Extrachromosomal expression of functional *Cannabis sativa* cannabidiolic acid synthase in *Phaedodactylum tricornutum*

Elisa Fantino [a,b,1], Anis Messaabi [a,1], Natacha Mérindol [a], Fatima Awwad [a], Nicolas Sene [a], Sarah-Eve Gélinas [a], Alexandre Custeau [a], Kimy-Li Rhéaume [a], Fatma Meddeb-Mouelhi [a,b], Isabel Desgagné-Penix [a,b,*]

[a] Department of Chemistry, Biochemistry and Physics, Université du Québec à Trois-Rivières, Trois-Rivières, QC, Canada
[b] Plant Biology Research Group, Université du Québec à Trois-Rivières, Trois-Rivières, QC, Canada

ARTICLE INFO

Keywords:
Microalgae
Cannabinoids
Biofactories
Diatoms
Metabolic engineering
Marine platform
Episome
Synthetic biology
Secretory pathway

ABSTRACT

Cannabis sativa's cannabidiolic acid (CBDA) offers significant therapeutic potential without inducing psychotropic effects but is typically found as part of a complex mixture of metabolites in plant extracts. Using a heterologous expression platform could allow the production of pure CBDA. Here, we propose to express CBDA synthase (CBDAS) in *Phaeodactylum tricornutum*. Episomes carrying *CBDAS* variants, incorporating the native signal peptide (CBDAS) or the highly abundant secreted protein 1 secretory signal peptide (SP:CBDAS) were constructed. *CBDAS* variants were tagged with the yellow fluorescent protein (YFP), introduced into the marine diatom, and screened by fluorescence. Confocal microscopy revealed that CBDAS and SP:CBDAS arranged in aggregated structures indicative of secretory pathway involvement. Western blot assays confirmed whole construct accumulation intracellularly, while soluble YFP was detected extracellularly. Finally, enzymatic assays showed CBDA production by both CBDAS and SP:CBDAS strains, confirming the potential of *P. tricornutum* as a platform for cannabinoid biosynthesis.

1. Introduction

Cannabis sativa-based preparations are prescribed in the USA and Canada to treat nausea following cancer chemotherapy, appetite loss due to acquired immune deficiency syndrome, and to provide symptomatic relief from neuropathic pain in multiple sclerosis patients [1]. Cannabinoids (CBs) are a group of metabolites long coveted for their psychoactive and medicinal properties [2–6]. Δ^9-Tetrahydrocannabinol (THC) and cannabidiol (CBD), as well as their carboxylated forms Δ^9-tetrahydrocannabinolic acid (THCA) and cannabidiolic acid (CBDA), are the potent CBs associated with the therapeutic benefits of *C. sativa* (*Cs*). CBD, in particular, has been reported to reduce sustained anxiety and improve sleep while being devoid of psychotropic effect [7–9]. *In planta*, cannabinoid and terpene biosynthesis pathways occur in secretory cells of the glandular trichomes of *C. sativa*. Both pathways utilize precursors such as geranyl pyrophosphate from the methylerythritol phosphate pathway and intermediate such as acetyl-CoA from fatty acid metabolism [10]. THCA and CBDA synthesis is catalyzed in the glandular trichome cavity by the THCA synthase (*Cs*THCAS) and the CBDA synthase (*Cs*CBDAS), respectively. Both secreted enzymes are members of the berberine bridge enzyme-like gene family, which contains a 28 amino acids (aa) N-terminal signal peptide and a flavin adenine dinucleotide (FAD) binding domain [11–13]. These FAD-dependent oxygenases catalyze the oxidative cyclization of cannabigerolic acid (CBGA), the last step of the major CB pathway. The structural and functional properties of *Cs*CBDAS are quite similar to those of *Cs*THCAS with 84 % identity in the amino acid sequences [11,14]. Both possess a disulfide bond and several N-glycosylation sites [12]. The main difference between the reactions they catalyze is the proton transfer step, *i.e.* *Cs*CBDAS extracts a proton from the methyl group at the end of CBGA to

Abbreviations: Au, absorbance units; CBD, cannabidiol; CBDA, cannabidiolic acid; CBDAS, cannabidiolic acid synthase; CBGA, cannabigerolic acid; EV, empty vector; ER, endoplasmic reticulum; FAD, flavin adenin dinucleotide; HA, hemagglutinin; HASP1, highly abundant secreted protein; OD, optical density; SP, signal peptide; THC, Δ9-tetrahydrocannabinol; THCA, Δ-9-tetrahydrocannabinolic acid; Thr, thrombine; YFP, yellow fluorescent protein.

* Corresponding author at: Department of Chemistry, Biochemistry and Physics, Université du Québec à Trois-Rivières, Trois-Rivières, QC, Canada.
E-mail address: Isabel.Desgagne-Penix@uqtr.ca (I. Desgagné-Penix).

[1] These authors contributed equally to the work.

https://doi.org/10.1016/j.algal.2024.103889
Received 13 October 2024; Received in revised form 12 December 2024; Accepted 29 December 2024
Available online 31 December 2024

yield CBD, while the *Cs*THCAS enzyme extracts a hydroxyl group to produce THC [14,15].

The isolation of pure CBD, desirable for its specific pharmaceutical properties, from *C. sativa* is challenging, as the extraction results in formulations containing hundreds of plant chemicals and minor cannabinoids [16,17]. Although there has been progress, its chemical synthesis has not been proven to be a cost-effective method either, mainly due to the complexity of its structure, resulting in high production and environmental costs, and suboptimal yields [18]. For these reasons, there is a need for alternative production platforms that are controlled and sustainable. To this aim, CBs pathway enzymes have been introduced in heterologous prokaryotic and eukaryotic hosts such as *E. coli* [19], yeast [20–24], model plants like *Nicotiana benthamiana* [25], filamentous fungi like *Penicillium chrysogenum* [26], and marine diatoms such as *Phaeodactylum tricornutum* [27,28]. These studies achieved variable yields of CBs and precursors, reaching up to hundreds of mg/L [29], and revealed that CBs are more suitable to be produced in eukaryotic compared to prokaryotic organisms. For instance, expression in *E. coli* cytosol failed to yield an active *Cs*THCAS [21]. The coding sequence of *CsTHCAS* fused to different signal peptides and tagged with the yellow fluorescent protein (YFP) was transiently heterologously expressed in *N. benthamiana* [25,30,31]. Interestingly, *Cs*THCAS enzyme was detected only when targeted to the endoplasmic reticulum (ER); while cytosolic and plastid localization resulted in no detectable protein [31]. Recent studies suggested that glycosylation and other post-translational modifications of *Cs*THCAS occurring in the ER might contribute to the correct folding of the enzyme and influence its stability [23,31].

Directing *Cs*THCAS or *Cs*CBDAS to specific intracellular compartments, such as the vacuoles, was also key to their function and CBs production in yeast [22–24,32]. These studies indicated that the expression and translocation of *Cs*THCAS and *Cs*CBDAS to specific intracellular compartments might result in the stabilization of the enzyme and increase their activity, possibly involving the pH-dependency of the reaction. Moreover, the translocation of the enzymes into specific compartments might shield the cells from the accumulation of CBs in the cytosol which was shown to be toxic to *C. sativa* protoplasts and *P. tricornutum* cell cultures [28,30]. Thus, an efficient *Cs*CBDAS heterologous platform would ideally allow for eukaryotic post-translational modifications through compartmentalization or secretion of the enzyme, or its product, and contain the necessary pathway precursors.

Microalgae are unicellular photosynthetic organisms emerging as heterologous hosts to produce plant specialized metabolites [33,34]. Diatoms are especially resistant to diverse environments and play an important role in fixing carbon from the ocean [35]. *P. tricornutum*, in particular, is known for its rapid growth rate and richness in fatty acids [36], and has been successfully used as a platform to produce lipids, terpenoids, and geraniol [37–40,58]. Recently, we demonstrated that diatom cell cultures could support *in vivo* production of the cannabinoid precursors olivetolic acid and CBGA following heterologous expression of tetraketide synthase and olivetolic acid cyclase [27,28]. Based on these characteristics, we hypothesize that *P. tricornutum* could be modified to efficiently biosynthesize CBDA.

This study aims to address these challenges associated with functional CBDAS heterologous expression and explore the suitability of producing CBDA in a sustainable and efficient manner. We engineered diatom strains with episomes containing three versions of the *CsCBDAS* sequence driven by the *P. tricornutum* endogenous promoter from the highly abundant secreted protein 1 (HASP1) [41,42]. The cassettes included 1) the native *Cs*CBDAS sequence, 2) a truncated sequence lacking the 28 aa N-terminal signal peptide (SP), and 3) a hybrid sequence, replacing the native SP with HASP1 18 aa secretory SP to direct *Cs*CBDAS to the extracellular matrix, mimicking enzymes behavior *in planta*. All sequences were codon-optimized for expression in the diatom and fused to YFP at the C-terminal, to easily follow protein accumulation and subcellular localization. After transformation, *P. tricornutum* strains harboring *CsCBDAS* complete sequence (CBDAS), truncated (Δ28aaCBDAS), and secreted version (SP:CBDAS) were characterized by flow cytometry, immunoblotting, confocal microscopy, and enzymatic assay. SP:CBDAS transconjugants yielded more clones with higher fluorescence compared to the other two designs. Both CBDAS and SP:CBDAS formed aggregate-like structures between the two plastid lobes, suggesting secretory pathway localization. Enzymatic assays confirmed that enzymes were active in both contexts, yielding CBDA as a product, whereas constructs without signal peptide were not active. The successful heterologous expression of *CsCBDAS* in *P. tricornutum* represents an important step in the development of microalgal-based biofactories for cannabinoid production. Moreover, our results reinforce the potential of the marine diatom, as a platform for efficient production of complex metabolites with pharmaceutical applications.

2. Results and discussion

2.1. Engineering P. tricornutum strains to express CsCBDAS

To metabolically engineer the brown algae *P. tricornutum* to biosynthetize CBDA, we designed three episomes harboring different versions of the gene encoding *Cs*CBDAS (Fig. 1A). Gene expression was driven from 499-bp of the *HASP1* promoter (HASP1p); followed by 1) a complete codon optimized *CsCBDAS* gene sequence (CBDAS), 2) a truncated version (Δ28aaCBDAS) without the secretory signal peptide (SP, 84 bp), or 3) the truncated version with an additional 54 bp from the 5′ coding sequence of *HASP1* (SP:CBDAS). Enzyme sequences were tagged with *YFP* and 3× hemagglutinin (HA) at their C terminal, linked by a thrombin cleavage sequence (LVPRGS) [43]. Three additional episomes were included as controls; the empty vector (EV) containing only the nourseothricin resistance cassette with the *nat* gene, a plasmid with the *YFP* reporter gene (YFP) under HASP1p, and one with *YFP* fused with the HASP1 SP (SP:YFP) at its N-terminal under HASP1p (Fig. 1A). These five constructs were successfully transformed into *P. tricornutum* by *E. coli* conjugation, and characterized for YFP signal, protein detection, and enzymatic assay (Fig. 1B).

Two weeks post-transformation, 36 colonies of each strain were randomly selected and grown in nourseothricin-containing plates for 10 more days, for a second antibiotic selection round. At that stage, colonies were screened by epifluorescence microscopy. The frequency of YFP^+ colonies, *i.e.* with higher fluorescence compared to the EV strain, was computed for each line (Table 1).

SP:CBDAS strain presented a higher percentage of YFP^+ colonies (50 %) compared to CBDAS (30.55 %) and Δ28aaCBDAS (19.44 %) strains (Table 1). Strains that presented fluorescence were grown in liquid culture for 10 days and further analyzed in a second screening round by recording YFP emission normalized on culture OD_{680} nm in a microplate reader, using EV strain as negative control (Figs. 2A, B; S1). Fluorescence was detected in YFP, SP:YFP, CBDAS, SP:CBDAS and Δ28aaCBDAS transconjugants, and SP:CBDAS clones displayed more fluorescence compared to CBDAS (One way Anova, Tukey post-test $p < 0.05$, Fig. 2A). A threshold equivalent to the mean background fluorescence detected in the EV clones, plus twice the standard deviation of that mean, was used to determine positive clones (Table 1, Fig. 2B). All three YFP and SP:YFP clones, used as positive controls, were fluorescent (Fig. 2A, B). Eight of the 11 clones of the CBDAS strain (72.7 %) remained fluorescent (Table 1). All tested clones from SP:CBDAS and Δ28aaCBDAS displayed YFP fluorescence above the threshold (Fig. 2B).

Thus, our results indicated that the constructs were successfully transformed and heterologously expressed by *P. tricornutum*, and that SP:CBDAS transconjugants presented a higher YFP fluorescence compared to CBDAS constructs. To some extent, these results are in contrast with Erdene-Ochir observations, which suggested that the addition of the SP signal to GFP decreased transcript levels compared to

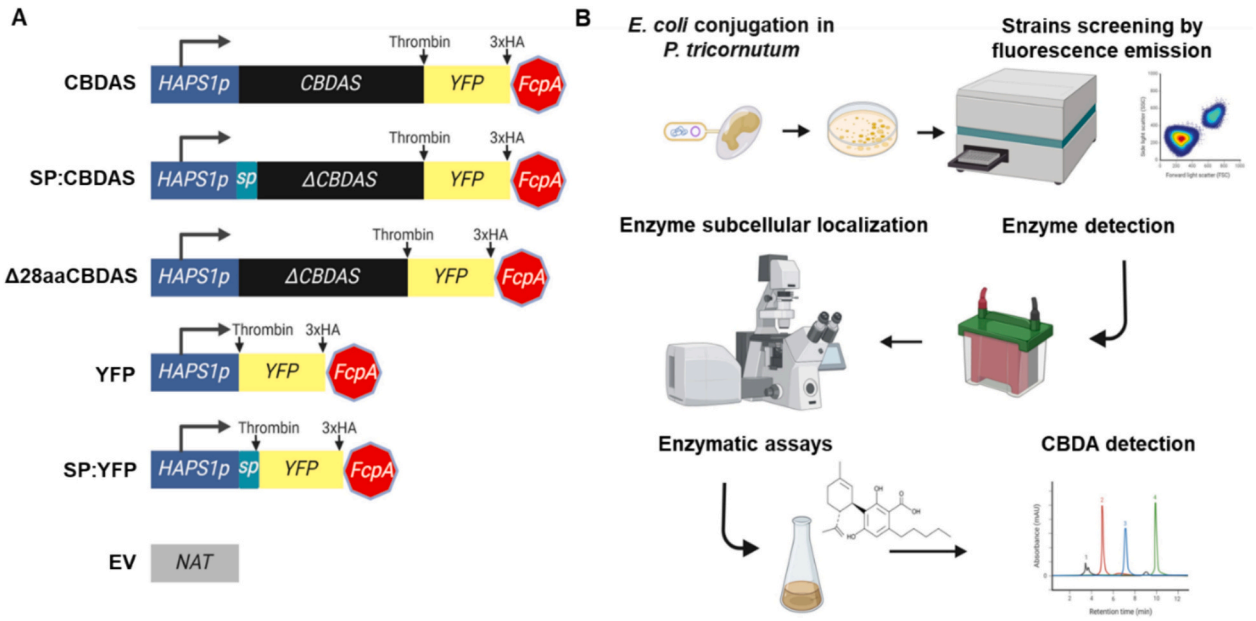

Fig. 1. Expression system and platform development. A. Scheme of the recombinant cassettes expressing cannabidiolic acid synthase (*Cs*CBDAS) driven by the diatom promoter *HASP1p* and tagged with the *yellow fluorescent protein* (YFP) reporter gene. Expression cassettes included the complete codon-optimized native sequence of *Cs*CBDAS (CBDAS), a truncated version (Δ28aaCBDAS), and a truncated version plus 54 bp from the 5′ coding sequence of *HASP1* (SP:CBDAS). All sequences were tagged in the C terminal with *YFP* and *3xhemagglutinin* (HA), linked to the enzyme by a thrombin cleavage sequence (LVPRGS). Moreover, three controls were used, *i.e. YFP* gene, SP:YFP both driven by HASP1p, and Empty vector (EV) encoding only the *nat* gene conferring nourseothricin resistance. B. Study workflow. *P. tricornutum* cells were transformed by *E. coli* conjugation, then clones were screened and analyzed by fluorescence emission in a microplate reader and flow cytometer, enzyme size was verified by immunoblotting assay and subcellular localization was observed in the confocal microscope. Enzyme activity was confirmed by the detection of CBDA on an HPLC-DAD. The figure was created with BioRender.com [44].

Table 1
Transconjugant strains screening by yellow fluorescent protein (YFP) fluorescence. Thirty-six randomly selected colonies of each strain, *Cs*CBDAS:YFP (CBDAS), *Cs*CBDAS fused to the HASP1 signal peptide (SP:CBDAS), and a truncated *Cs*CBDAS version without the first 28 aa (Δ28aaCBDAS) were screened under a fluorescence microscope. YFP^+ clones selected from the first screen were grown in L1 liquid media for 10 days in 96-well plates, and YFP fluorescence was analyzed with a microplate reader (second screen). Empty vector (EV) strain was used as a negative control to settle the basal autofluorescence.

Strain	1st screening YFP^+ clones (Fluorescence microscopy)	2nd screening YFP^+ clones $(Ex_{500}Em_{539})/OD_{680}$ nm
CBDAS	30.6 % (n = 11/36)	72.7 % (n = 8/11)
SP:CBDAS	50 % (n = 18/36)	100 % (n = 18/18)
Δ28aaCBDAS	19.4 % (n = 7/36)	100 % (n = 7/7)

GFP alone constructs [41]. The authors suggested that the presence of the SP sequence could affect the steady-state level of GFP mRNA. In our study, the addition of the SP signal had a positive impact at the fluorescence level, but we used different constructs, and episomal expression rather than randomly integrated genomic expression, limiting our ability to compare with Erdene-Ochir et al. [41].

2.2. Characterization of the selected fluorescent clones

Three clones with the highest fluorescence for each strain were selected for further characterization. The culture growth curves and YFP fluorescence were registered for 14 days and compared to the EV strain (Fig. 3A and B). Strains presented a similar pattern, showing that the presence of the transgene did not negatively affect the growth of *P. tricornutum* cells. The YFP fluorescence increased from day 7, as shown before [41,42] [35,36], with clone SP:YFP 13 showing the highest level at day 14.

Clones were then analyzed on a flow cytometer at day 10 (Fig. 3C). The EV strain was used as a negative control. YFP clones 3, 7, and 11 presented 35.4 %, 55.9 %, and 36.7 % of YFP^+ cells, respectively, while SP:YFP clones 4, 13, and 17 showed 79.7 %, 48.2 %, and 44.6 % of YFP^+ cells. The selected CBDAS clones (7, 11, and 18) and SP:CBDAS (2, 6, and 8) showed similar frequency of YFP^+ cells; 26.7 %, 37.6 % and 36.1 % *vs.* 43.2 %, 36.6 % and 26.5 %. Regarding Δ28aaCBDAS, clone 10 presented a cell population with a lower percentage (9.23 % of YFP^+ cells), compared to clones 1 and 28, with 50.9 %, and 41.7 %, respectively. These results are consistent with George *et al*, showing that episomal expression is an efficient method to generate *P. tricornutum* transconjugants that express transgenes, requiring less screening compared to random integration methods [40].

2.3. Subcellular localization of CBDAS in P. tricornutum transconjugants

To assess the subcellular localization of CBDAS from the three constructs, *i.e.* without SP (Δ28aaCBDAS), with endogenous SP (CBDAS), and with HASP1 SP (SP:CBDAS), transconjugants were visualized on a confocal microscope, acquiring YFP fluorescence (yellow), and chlorophyll autofluorescence (red) using EV, YFP and SP:YFP as controls (Fig. 4). YFP fluorescence in the YFP control strain was visible throughout the cytoplasm at the early stationary phase (day 10). As previously observed, the HASP1 SP caused considerable changes in the subcellular localization of YFP, clustering in the chloroplast ER rather than the cytoplasm, as a clustered dotted structure between the two plastid lobes [41,45–47]. According to Erdene-Ochir *et al*, this suggests that the HASP1 signal peptide leads to YFP entry into the secretory pathway. Interestingly, both CBDAS and SP:CBDAS strains presented a localization pattern consistent with clustered structure between the plastid lobes, similar to SP:YFP (Figs. 4, S2 and S3). CBDAS fluorescence pattern also corresponded to the signal of the medial Golgi marker protein XylT [47]. A similar pattern was observed when the potential retromer subunit Vps29, the structure involved in endosomal retrograde

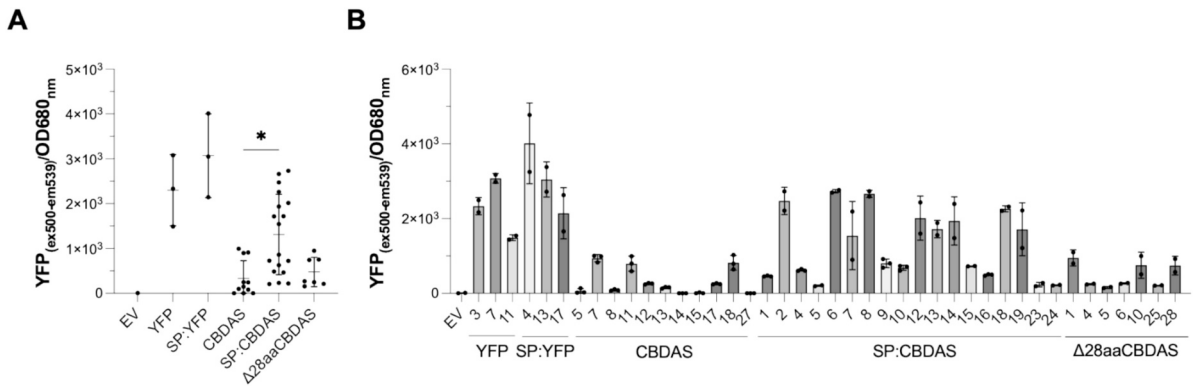

Fig. 2. CBDAS strains screening for YFP fluorescence. The strains selected by the fluorescence microscope were transferred to liquid media where the YFP fluorescence intensity was measured by the microplate reader, normalized to the OD680 nm, and compared with EV strain autofluorescence (A). Mean ± SD; $n = 3$ biologically independent samples for each strain were plotted. The clones with a YFP fluorescence higher than the EV fluorescence (mean + (SD) × 2) were determined as YFP positive (B). A One way Anova with Tukey post-test was performed (*$p < 0.05$).

transport to the Golgi apparatus, was heterologously expressed in *P. tricornutum*. These results suggest that CBDAS and SP:CBDAS both localized in the secretory pathway. Unexpectedly, the soluble version of Δ28aaCBDAS enzyme did not behave as a cytosolic protein, although more diffuse than CBDAS and SP:CBDAS, aggregates were observed close to the plastid (Figs. 4 and S4), in all three clones.

Overall, the localization pattern of SP:CBDAS and CBDAS suggests that they cluster in the chloroplastic ER, where post-translational modifications like N-glycosylation, required for activity, stability, and correct folding of endogenous as well as transgenic enzymes, occur [48].

2.4. CBDAS accumulation and secretion

To analyze the impact of HASP1 signal peptide on enzyme secretion into the extracellular matrix, we performed a western blot using protein pellets from cell extracts and supernatants from stationary phase cultures (Fig. 5A & B). As expected, the EV protein extract did not show any bands following immunoblotting with anti-YFP (Fig. 5A), while the positive control (10 ng of purified GFP) showed the predicted band at 27 kDa. YFP clones presented the expected band at 32 kDa (Thr:YFP:3HA) and a band below it (~30 kDa). The YFP clone 11, presented both bands, but the upper band showed higher intensity. In the case of the SP:YFP strains, clones showed the expected band (~34 kDa, SP:Thr:YFP:3HA), with additional smaller bands at high intensity for clone 4. For further assays, clones YFP 7 and SP:YFP13 were used. All cell extracts from CBDAS clones and SP:CBDAS produced proteins of the predicted size of 92–93 kDa, confirming intracellular accumulation. When Slattery et al. heterologously expressed the receptor-binding domain of the SARS-CoV-2 spike protein, under a longer version of HASP1p containing the secretory signal (642-bp), only one of the 9 selected clones produced the desired protein [36]. In our study, the fusion of CBDAS to an endogenous and recognized signal peptide by the secretory mechanism could stabilize the enzyme, as proven when targeted to the ER [31]. To verify, if CBDAS and SP:CBDAS were secreted, the extracellular media was concentrated 250 times, and analyzed by western blot (Fig. 5B). YFP clone 7 and EV strains supernatants were used as controls and no specific band was detected. However, SP:YFP, CBDAS, and SP:CBDAS displayed bands close to YFP size (~27 kDa), but CBDAS:YFP was not detected. Uncropped blot and red ponceau stain are shown in Fig. S5.

Thus, we could not detect CBDAS and SP:CBDAS in the extracellular media, only the YFP cleaved portion was visible. The detection of YFP in the extracellular is consistent with Erdene-Ochir et al., which detected secreted GFP from SP:GFP constructs by western blot during the stationary phase [49]. The absence of detection of the enzymes could be due to degradation during the secretion process, and/or cleavage from YFP. Studies of protein production in yeast showed that when cells reached their maximal secretory adaptation capabilities, the subset of high protein accumulator cells trigger protein degradation in the entire cell population, or transiently experience a secretion burnout [50]. Alternatively, a cleaved tag-free version of CBDAS could be present in the extracellular matrix but would remain undetectable. A previous study has suggested that the thrombin cleavage sequence could be recognized and cleaved in *P. tricornutum* [51].

2.5. CBDAS enzymatic activity

As the enzyme was detected in the cell extracts but not in supernatant, cell lysates were used to assess the activity of CBDAS transconjugants, similarly to Slattery et al. [42].

Clones were scaled up from the L1 agar plate colonies obtained after *E. coli* conjugation, to avoid possible mutations generated by continuous transfers [52]. The percentage of YFP^+ cells was measured in cell cultures grown to the stationary phase for 21 days (Fig. 6A). Total soluble protein was extracted from fluorescent CBDAS 7, 11, 18, SP:CBDAS 2, 6, 8, Δ28aaCBDAS clones 1, 10, 28, EV, YFP clone 7, and SP:YFP clone 13 transconjugants and used for enzymatic assay without protein purification, to avoid protein degradation. CBGA was used as a substrate, and the products of the reaction were analyzed and identified by HPLC-DAD (Figs. 6B, S5, S6). Neither CBDA nor any other traces of CBs were detected in cell protein extracts of SP:YFP and Δ28aaCBDAS strains. A signal eluting at 8.827 min corresponding to the CBDA standard was detected when CBDAS and SP:CBDAS transconjugants protein extracts were incubated with CBGA as substrate. The UV spectrum of the *in vitro* assay was also compared with the one of authentic reference standard CBDA (Fig. S7) and then the identification was confirmed by HPLC-MS/MS (Fig. S8). The highest yield corresponding to 0.55 mg/L of CBDA was obtained in SP:CBDAS clone 6 cell protein extract. Thus, both constructions, with endogenous signal peptide (CBDAS) and HASP1 signal peptide (SP:CBDAS) led to the *in vitro* production of CBDA, while removing the signal peptide abolished the enzyme activity. These results add to the growing evidence that the enzyme CBDAS requires to be processed through the secretory pathway. It also adds to our previous studies suggesting that the diatom is a suitable host for CBs production [27,28].

The first report of CBDAS heterologous production was published in 2018, using wild-type and mutant enzymes heterologously expressed in *Komagataella phaffii* [53]. The mutant strain CBDAS A414V + A46V + T47A was able to produce 0.42 $g.L^{-1}$ CBDA and 0.13 $g.L^{-1}$ of THCA when supplemented with CBGA [23], increasing CBDAS catalytic activity by 3.3 times [23]. In 2019, Luo et al. generated strains of *S. cerevisiae* that produced different CBs from galactose. The highest reported titers of CBDA by hexanoic acid supplementation were 4.3 μg.

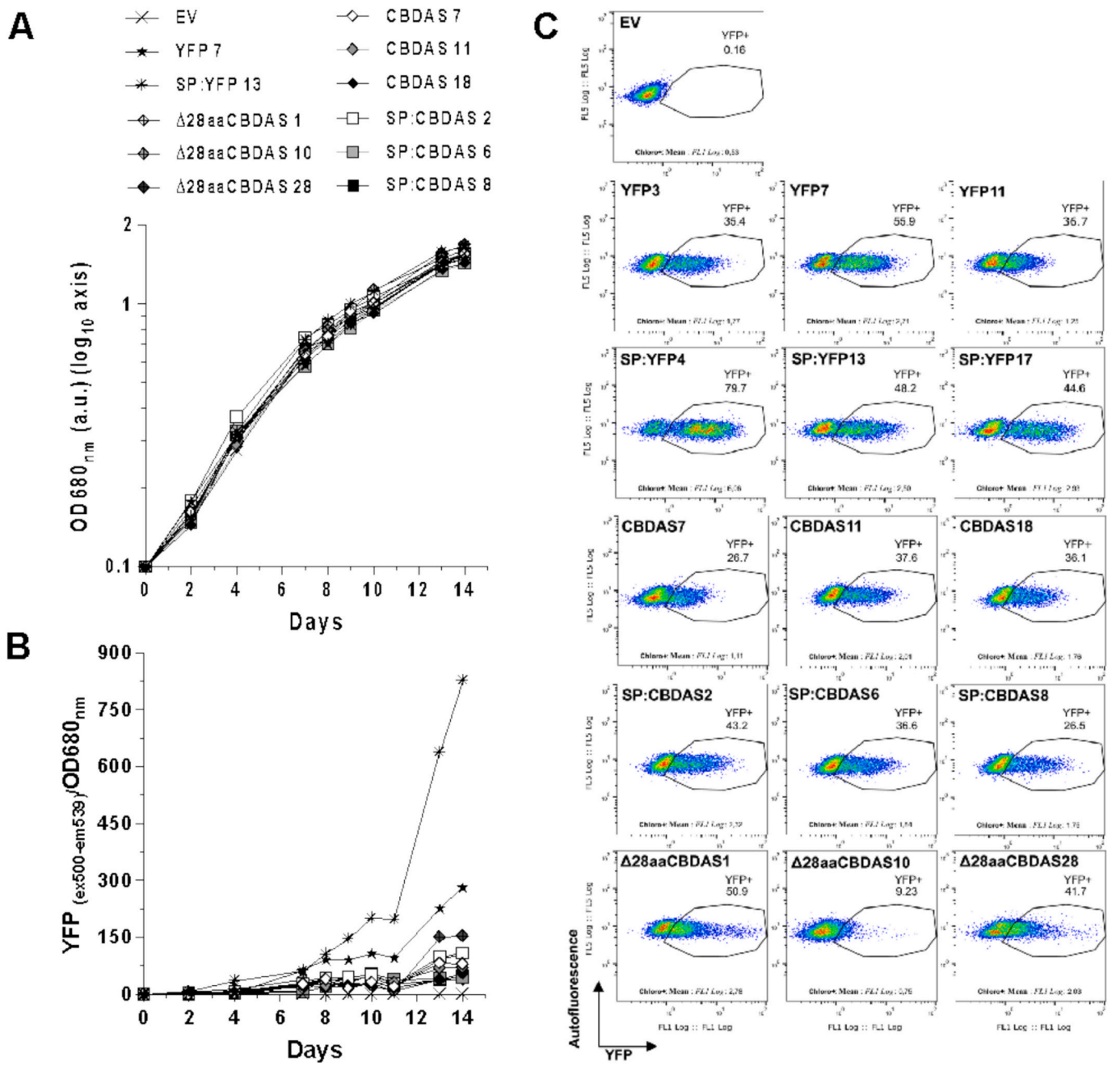

Fig. 3. Characterization of the selected transconjugants. A. Growth curves of each strain, the optical density (OD) at 680 nm was followed for 14 days. B. YFP fluorescence emission (excitation 500 nm-emission 539 nm) was measured and normalized to the OD for the 12 cultures monitored in A. C. Representative dot plots of 3 selected clones of each strain. Pseudo-color dot plots of empty vector (EV) and transformants strains; YFP fluorescence was detected at 530 nm on the x-axis, and autofluorescence at 448 nm on the y-axis. Gates and frequencies of total YFP populations were designed according to the autofluorescence of the negative control EV shown as a reference.

L^{-1} CBDA [24]. A second group successfully implemented *de novo* biosynthesis of CBD in *S. cerevisiae*, yielding 6.92 mg/L, by over-expressing the bile pigment transporter 1, which efficiently transfers CBGA from the cytoplasm to the vacuole, where catalysis takes place [15]. Experiments in *S. cerevisiae* with co-overexpression of WT *Cs*CBDAS and transcription factor HAC1, which activates the unfolded protein response to restore ER homeostasis [54], resulted in increased specific activities of 11-fold, as determined by *in vitro* assays [32]. Moreover, multiple copies of *Cs*CBDAS were integrated using a multi-copy integration system, and the resulting strain produced 0.13 mg/L CBDA at pH 4 [32]. Overall, the heterologous expression systems for CB production still require optimization and fine-tuning to be profitable to the industry. However, these studies indicate several avenues for further optimization of *Cs*CBDAS activity in *P. tricornutum*.

Here, we succeeded in engineering the diatom *P. tricornutum* with an active CBDAS, showing the importance of its localization in the ER through the encoded signal peptide. This work highlights the importance of studying linkers and signal peptide behavior in new heterologous platforms, such as the diatom *P. tricornutum*, as well as characterizing the secretory network to construct more efficient tools.

Future research should include the evaluation of medium optimization (phosphate and iron deprivation) [42], directed mutagenesis, the use of smaller tags, different sequence of linkers [51], and increasing the gene copy number on CBDA titers in *P. tricornutum*. In addition,

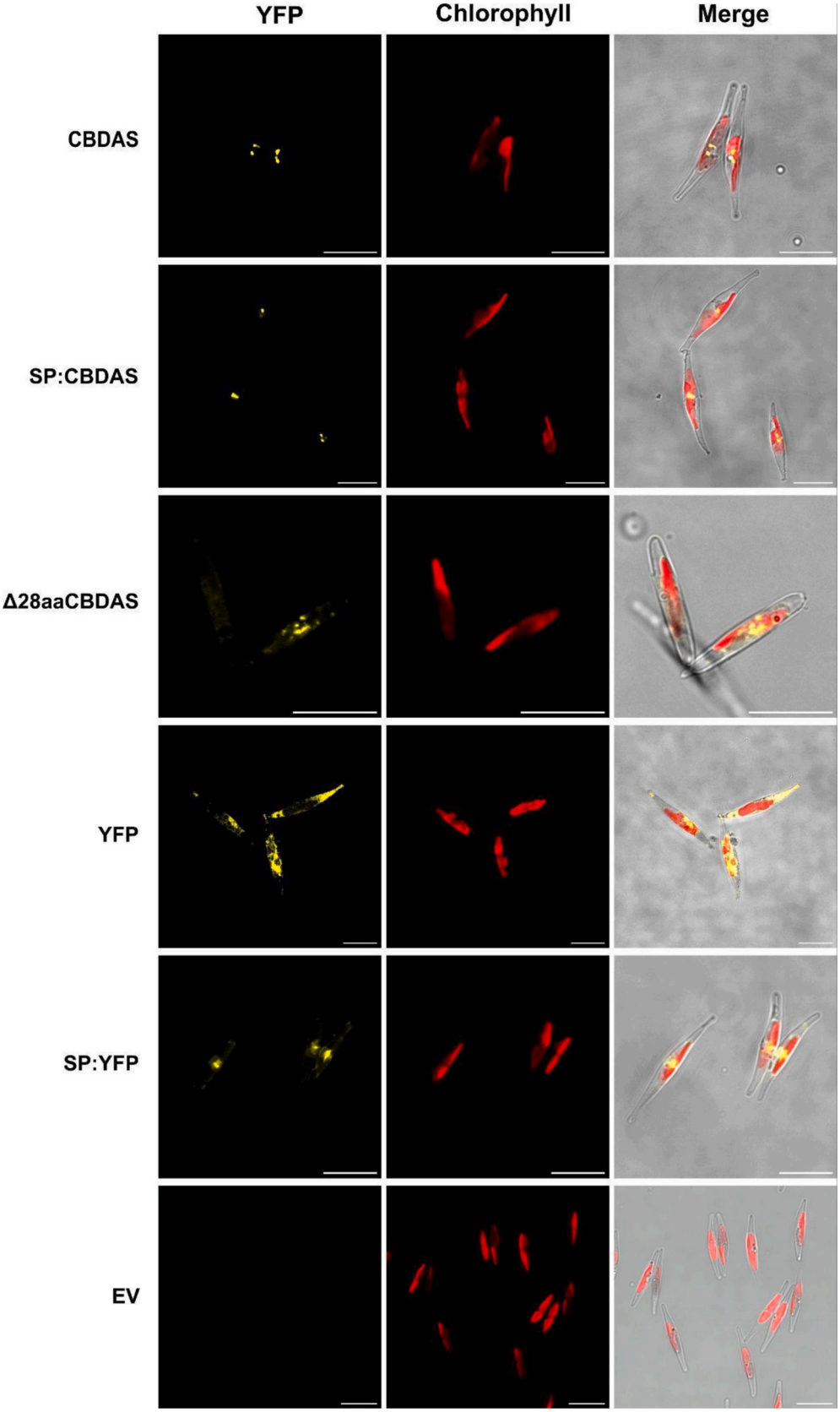

Fig. 4. SP:CBDAS and CBDAS localize at the chloroplastic endoplasmic reticulum in *P. tricornutum* transconjugants. YFP fluorescence, chlorophyll autofluorescence, and the merging of three fields are shown in transgenic lines producing CBDAS:YFP, SP:CBDAS:YFP, Δ28aaCBDAS:YFP, SP:YFP, and YFP were visualized by confocal laser microscopy. YFP and EV cells were used as positive and negative controls. Scale bars = 10 μm.

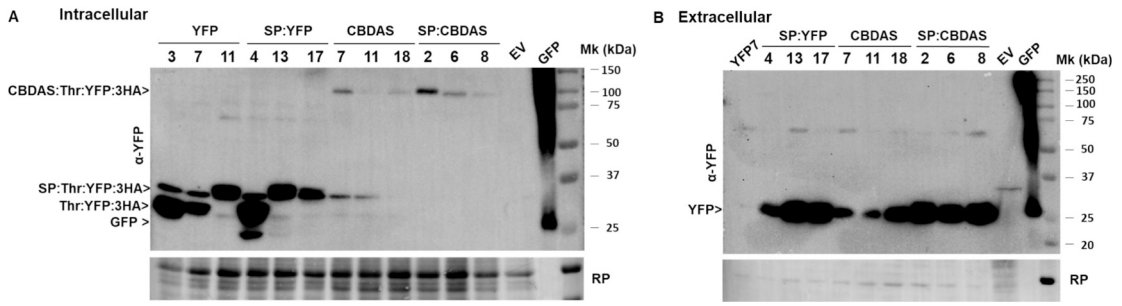

Fig. 5. CBDAS protein detection. Western blot analysis using anti-YFP antibody of total intracellular protein extract from cell lysate and extracellular culture. (A) Cell lysates and (B) culture supernatants. YFP (Thr:YFP:3HA, 32 kDa), SP:YFP (SP:Thr:YFP:3HA, 34 kDa), CBDAS (CBDAS:Thr:YFP:3HA, 93 kDa), SP:CBDAS (SP:CBDAS: Thr:YFP:3HA, 92 kDa), EV and purified GFP/YFP (27 kDa). Lower panel, stained blot with red ponceau solution (RP). Full-length Western blots are presented in Supplementary Fig. S5.

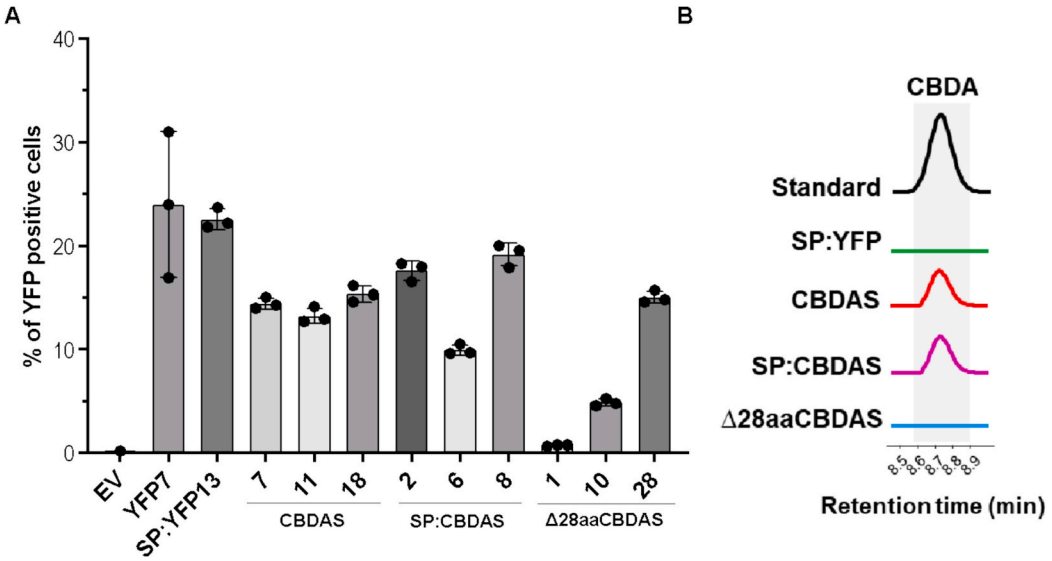

Fig. 6. *P. tricornutum* transconjugants display CBDAS activity. A) Percentage of YFP^{+} cells of selected transconjugants after 21 days of culture. B) HPLC-DAD chromatograms of *in vitro* CBDA production. Extracts were analyzed by HPLC-DAD and signals were compared to authentic CBDA standard (Figs. S6, S7, S8, and S9).

strategies to reduce CBs cytotoxicity in *P. tricornutum* cells [28] such as cell compartmentalization and the use of cannabinoid transporters must be considered.

3. Conclusion

We previously demonstrated the use of *P. tricornutum* as an *in vivo* heterologous production platform for olivetolic acid and CBGA, precursors of cannabinoids. In the present study, we report, for the first time, the production of one of the most critical enzymes in the cannabinoid biosynthetic pathway in microalgae. Our results showed that the production of three versions of CBDAS *i.e.* native, modified with an endogenous secretory signal peptide, and truncated one, can be produced in *P. tricornutum*. The YFP fluorescence-based screening method enabled high-throughput clone selection and facilitated the detection of high fluorescence in the constructs driven by the HASP1 promoter. Enzymatic assays confirmed the activity of CBDAS, with CBDA as the product in both the native and secretory constructs. Overall, we demonstrated that CBDA production through the heterologous expression of CBDAS in *P. tricornutum*, achieves competitive levels when compared to yeast platforms. Although additional improvements are required, these findings validate the diatom as a platform for cannabinoid biosynthesis, offering a sustainable and scalable alternative to traditional production systems.

4. Methods

4.1. Plasmids construction

Plasmids were constructed by Gibson assembly using the NEBuilder® HiFi DNA Assembly Bundle for Large Fragments (New England Biolabs, Canada). Amplicons used for assemblies were amplified by PCR with PrimeSTAR GXL DNA Polymerase (Takara Bio, Japon) following the manufacturer's protocol. Plasmid pPtGE31 is used as a template to construct the expression vectors [55]. The *C. sativa CBDAS* gene was fused in the C terminal to the YFP gene, linked by thrombin cleavage sequence, and a 3xHemagglutinin (HA) tag was introduced in the C terminal of the *YFP* gene. All the sequences were codon optimized for *P. tricornutum* and synthesized by Bio Basic (Markham, Ontario, Canada). These sequences were introduced in the expression cassette containing the 499 bp '*Highly abundant secreted protein 1*' (*HASP)1* promoter [41] and *FcpA* terminator. *N-acetyltransferase* gene (*nat*) conferring resistance to Nourseothricin was used as a selection marker, under *FcpC* promoter and *FcpC* terminator. As a result, the following plasmids were generated; the *CBDAS* complete codon sequence, *HASP1pro:CBDAS:Thr:YFP:3HA* (CBDAS), a truncated *CBDAS* version without 84 bp from the 5′, *HASP1pro:Δ84CBDAS:Thr:YFP:3HA* (Δ28aaCBDAS) and the truncated *CBDAS* version with the endogenous HASP1 signal peptide SP, 54 bp in the 5′, *HASP1pro:SP54:Δ84CBDAS:Thr:YFP:3HA* (SP:CBDAS). As a control, *Thr:YFP:3HA* sequence (*YFP*) and *SP:Thr:YFP:3HA* sequence

with the signal peptide *SP (SP:YFP)*. To enhance protein production, a minimal Kozak sequence was placed directly before each ATG initial codon. A modified version of the pPtGE31 vector [56], harboring *nat* gene cassette, was used as a negative control. All DNA sequences and primers used in this study are listed in Supporting Information Table S1 and S2 respectively.

4.2. Microbial strains, growth conditions and transformation

Escherichia coli (NEB® 10-beta, New England Biolabs, Canada) were grown in Luria Broth (LB) supplemented with appropriate antibiotics (chloramphenicol, 30 mg/L). Plasmids were extracted using a miniprep kit allowing the extraction of large vectors (Biobasic EZ10 miniprep kit, NY, USA), sequenced by CCIB DNA Core (Massachusetts General Hospital, United States of America) through Next-Generation sequencing platform and then amplified in Epi 300 strain containing pTA-MOB plasmid to allow conjugation with diatoms, as described in the literature [56]. Briefly, 1 mL of wild-type *P. tricornutum* was seeded on 0.5× L1, 1 % agar plates and grown at 18 °C on a light/dark cycle of 16/8 h for 4 days. Before transformation, 1 mL of L1 media was added to each agar plate, cells were scraped and recovered by pipetting in a sterile tube. Cell concentration was then adjusted to 5.0×10^8 cells/mL. A volume of 25 mL *E. coli* culture containing the assembled plasmid and pTA-MOB was grown at 37 °C under agitation to OD600 of 0.8, then centrifuged at 3000 x*g* for 10 min and resuspended in 250 μL of SOC media. Conjugation was initiated by adding 200 μL of *P. tricornutum* to 200 μL of *E. coli* cells. The cell mixture was plated on 0.5× L1, 5 % LB, ~1 % agar plates, incubated at 30 °C for 90 min in the dark, and transferred to 18 °C in the light and grown for 2 days. After the recovery period, 1 mL of L1 media was added to the plates to collect cells by scraping. Then, cells were plated on 0.5 X L1, 1 % agar plates supplemented with nourseothricin 200 mg/L for selection and incubated at 18 °C. Transformed colonies appeared after 2 weeks.

4.3. Strains selection

Thirty-six clones per construct were plated on new selective media supplemented with nourseothricin 200 mg/L. After 10 days colonies were observed with a magnification of 80 to 120× and screened by fluorescence under a Fluorescent Stereo Microscope Leica M165 FC with GFP filter. Then, 200 μL cell culture of the selected strains was analyzed in the Synergy H1 BioTek microplate reader to measure the YFP fluorescence at Ex/Em wavelengths of 500/539 nm ($n = 3$) and OD680nm. EV and YFP strains were used as negative and positive controls, respectively. Strains with fluorescence higher than the mean ratio ($[Ex_{500}/Em_{539}]/OD_{680}$) + 2 x [SD] of EV were determined as YFP positive and analyzed with a CytoFLEX S flow cytometer (Beckman) equipped with violet (405 nm), blue (488 nm), yellow-green (561 nm) and red (638 nm) lasers. In this case, 75 μL of 10-day-old cultures were filtered and transferred to clear 96-well plates with 200 μL of L1 in each well. Chlorophyll autofluorescence was detected in the PerCP channel (690/50 nm), while YFP fluorescence was detected in the FITC channel (525/40 nm). Figures and statistics were analyzed using BD FlowJo version 10 software (BD Biosciences, La Jolla, CA, USA, 2020).

4.4. Protein extraction

Fifty mL of bioengineered strains were grown for 21 days in L1 media containing nourseothricin (200 mg/L) then centrifuged at 3500 ×*g* for 15 min at 4 °C. The supernatant was kept and concentrated 200× using Amicon Ultra-15 30 K Centrifugal Filter Units from Sigma (cat. #UFC903008). Pellets were weighed and protein extraction was performed according to Fantino et al. [28]. Concentrated supernatants containing soluble protein fraction were kept at −20 °C for further use in western blot. Total protein samples were quantified using RC DC™ Protein Assay Kit I (Bio-Rad cat # 5000121).

4.5. Western blot

For each clone, 60 μg of total proteins were loaded in 10 % SDS-PAGE. Transfer settings: 80 V until proteins went through the stacking gel, then at 120 V for 2 h were used. Primary antibodies were incubated overnight at 4 °C. Primary anti-GFP/YFP/CFP and anti-HA from Cedarlane (Ontario L7L 5R2 Canada, cat. #CLH106AP) and ThermoFisher Scientific (Illinois 61101 USA, cat. #MA1-21316) respectively. Both were used at a 1:1000 dilution in 3 % BSA. After three washes with TBST solution, the blots were incubated for 1 h in a 1:20,000 dilution, of Immun-Star Goat Anti-Mouse (GAM)-HRP Conjugate from Bio-Rad (Ontario L5T 1C9 Canada, cat. #1705047) in 5 % milk. Purified GFP (10 ng) and Multiple Tag (10 ng), from GenScript (cat. #M0101) were used as a positive control for YFP and HA Tag. After three washes with TBST solution, protein detection was realized by using Clarity Max Western ECL Substrate-Luminol solution from Bio-Rad (cat #1705062S). Chemiluminescence detection and Red Ponceau stained (Glacial Acetic Acid 5 % *v*/v, Ponceau Red dye 0.1 % m/v) of the blots were visualized using ChemiDoc Imaging System with Image Lab Touch Software (Bio-Rad cat # 12003153) and Image Lab™ Software (Bio-Rad cat # 1709690).

4.6. Confocal microscopy

Live cell Images were captured, and protein localization was visualized with a Leica TCS SP8 confocal laser scanning microscope (Leica Microsystems) with a 40×/1.30 oil immersion objective. The YFP excitation wavelength used was 488 nm and the emission of fluorescence signals was detected from 500 to 525 nm. Chlorophyll autofluorescence was observed with an excitation wavelength of 552 nm and the emission of fluorescence signals was detected from 630 to 670 nm. The combined images were generated using Leica Las X software.

4.7. CBDAS in vitro enzymatic assay

Enzymatic assays were carried out using 500 μg of total protein extraction, from 3 biologically independent samples, in a 200 μL volume reaction. The reaction was adapted from Valliere et al. [57], composed of (pH 4.5), 25 mM $MgCl_2$, 25 mM KCl, 250 μM FAD, and 300 uM CBGA, and incubated ON at 30 °C. The reactions were then extracted with 3 volumes of methanol. Metabolite extracts were filtered (0.2 μm PTFE, Agilent Technologies, cat. no. 5190-5265), then dried in a SpeedVac concentrator and resuspended in 100 μL methanol, HPLC grade, and stored at −20 °C for high-performance liquid chromatography coupled with diode-array detection (HPLC-DAD) analyses. Metabolite detection was confirmed by HPLC coupled with tandem mass spectrometry (MS/MS).

4.8. Cannabinoids and precursors standards

Olivetolic acid (OA, CAS 491-72-5) and olivetol (OL, CAS 500-66-3) were purchased from Santa Cruz Biotechnologies (Dallas United States). Delta-9-tetrahydrocannabinol (THC, CAS 1972-08-3), cannabidiol (CBD, CAS 13956-29-1), cannabinol (CBN, CAS 521-35-7), Δ-9-tetrahydrocannabinolic acid (THCA, CAS 23978-85-0), cannabidiolic acid (CBDA, CAS 1244-58-2), cannabigerolic acid (CBGA, CAS 25555-57-1), cannabichromene (CBC, CAS 20675-51-8), cannabigerol (CBG, CAS 25654-31-3), tetrahydrocannabivarin (THCV, CAS 31262-37-0) and cannabidivarin (CBDV, CAS 24274-48-4) were purchased from Agilent Technologies (QC, Canada). Cannabinolic acid (CBNA, CAS 2808-39-1) was purchased from Sigma-Aldrich (ON, Canada).

4.9. HPLC-DAD and HPLC-MS/MS analysis

Analyses were conducted using high-performance liquid chromatography (HPLC) with diode-array detection (DAD). Chromatographic

separation of analytes was performed using an InfinityLab Poroshell 120 EC-C18 column (4.6 × 100 mm, 2.7 mm; Agilent Technologies, QC, Canada) maintained at 30 °C. Ten microliters of the sample were injected into the analytical device. Mobile phases used during analysis were made of (A) formic acid 0.1 % *v*/v in milli-Q water and (B) formic acid 0.1 % v/v in methanol with a flow rate of 1 mL/min. The HPLC gradient program was set as follows: 0 min, 70 % B; 1.0 min, 70 % B; 6.0 min, 77 % B; 15.0 min, 90 % B; 15.1 min, 70 % B and 18.0 min, 70 % B. The total run time per sample was 18.5 min to allow the reconditioning of the column before the next injection. The diode array detector was set to acquire the wavelength range of 190 to 400 nm with a deuterium (D2) lamp. All the analyses were done using a UV wavelength of 220 nm. Compounds were identified by comparing retention time and maximum absorption wavelengths obtained with the ones of reference standards (Table S3). Standard calibration curves were prepared as follows to allow absolute quantification; two working solutions were prepared containing CBGA and CBDA at 10 mg/L and 100 mg/L each in HPLC grade methanol. These solutions were further diluted to prepare calibration solutions with the following concentrations in triplicate: 0.5, 1, 2, 4, 5, 10, 25, 50, and 100 mg/L. These standard solutions were injected into the HPLC-DAD system and used to generate calibration curve regressions. Fig. S1 shows the calibration curves obtained by plotting the area under the curve obtained as a function of the analyte's concentration. This allowed CBGA and CBDA quantification for the enzymatic and supplementation assays. Confirmatory analyses were performed using high-performance liquid chromatography (HPLC) coupled with tandem mass spectrometry (MS/MS) (Agilent, QC, Canada). This system has an Agilent Jet Stream ionization source, a binary pump, an autosampler, and a column compartment. Compound separation was achieved using an InfinityLab Poroshell 120 EC-C18 column (4.6 × 100 mm, 2.7 mm; Agilent Technologies, QC, Canada). *In vitro* and supplementation assays samples were centrifuged for 10 min at 12,000 rpm and diluted 10-fold in the mobile phase (*i.e.*, formic acid 0.1 % *v*/v in milli-Q water and formic acid 0.1 % v/v in methanol (30:70)). Five µL of each sample were injected onto the column that was set at 50 °C. A gradient method made of (A) formic acid 0.1 % v/v in milli-Q water and (B) formic acid 0.1 % v/v in methanol with a flow rate of 0.5 mL/min was used to achieve chromatographic separation. The HPLC elution program was as follows: 0 min, 70 % B; 7.0 min, 100 % B; 10 min, 100 % B; 12.0 min, 70 % B. The total run time was 14 min per sample. The parameters used in the MS/MS source were set as follows: gas flow rate 8 L/min, gas temperature 220 °C, nebulizer 55 psi, sheath gas flow 12 L/min, sheat gas temperature 380 °C, capillary voltage 4500 V and nozzle voltage 0 V. Agilent MassHunter Data Acquisition (version 1.2) and MassHunter Qualitative Analysis (version 10.0) softwares were used for data acquisition and processing respectively. Samples analyses were carried out in triggered multiple reaction monitoring (tMRM) acquisition mode allowing compound identification using authentic standards. Table S4 shows MRM transitions and MS/MS parameters used for targeted compound identification.

4.10. Statistics and reproducibility

General data analysis (means and standard deviation) was performed primarily by GraphPad Prism 10.0.2. All experiments were performed with three biological replicates and values were expressed as means ± standard errors.

CRediT authorship contribution statement

Elisa Fantino: Writing – review & editing, Writing – original draft, Visualization, Validation, Methodology, Investigation, Formal analysis, Data curation, Conceptualization. **Anis Messaabi:** Writing – review & editing, Writing – original draft, Visualization, Validation, Methodology, Investigation, Formal analysis, Data curation, Conceptualization. **Natacha Mérindol:** Writing – review & editing, Visualization, Project administration, Data curation. **Fatima Awwad:** Writing – review & editing, Writing – original draft, Formal analysis. **Nicolas Sene:** Writing – review & editing, Writing – original draft, Formal analysis. **Sarah-Eve Gélinas:** Writing – review & editing, Methodology, Investigation, Formal analysis. **Alexandre Custeau:** Writing – review & editing, Investigation, Formal analysis. **Kimy-Li Rhéaume:** Writing – review & editing, Investigation, Formal analysis. **Fatma Meddeb-Mouelhi:** Writing – review & editing, Supervision, Project administration, Conceptualization. **Isabel Desgagné-Penix:** Writing – review & editing, Supervision, Resources, Project administration, Funding acquisition, Conceptualization.

Declaration of competing interest

The authors declare the following financial interests/personal relationships which may be considered as potential competing interests: Isabel Desgagne-Penix reports financial support was provided by Natural Sciences and Engineering Research Council of Canada. Isabel Desgagne-Penix reports financial support was provided by Mitacs Canada. Isabel Desgagne-Penix has patent issued to Algea-C. If there are other authors, they declare that they have no known competing financial interests or personal relationships that could have appeared to influence the work reported in this paper.

Acknowledgments

Special thanks to Professor Hugo Germain and MSc. Mélodie B. Plourde from the Université du Québec à Trois -Rivières for providing us with the purified GFP to use as a control for immunoblotting of Fig. 4. We acknowledge that financial support for this research was funded by the Natural Sciences and Engineering Research Council of Canada through the Alliance program Award No ALLRP 570476-2021 to IDP. Additional support in the form of scholarships to EF, AM, FA, NS, K-LR, and AC from Mitacs-Acceleration/Globalink program grants no IT12310, IT16463, and IT19432 to IDP is also acknowledged.

Appendix A. Supplementary data

Supplementary data to this article can be found online at https://doi.org/10.1016/j.algal.2024.103889.

Data availability

Data will be made available on request.

References

[1] J. Castillo-Arellano, et al., The polypharmacological effects of cannabidiol, Molecules 28 (2023) 7.
[2] N. Stella, THC and CBD: similarities and differences between siblings, Neuron 111 (3) (2023) 302–327.
[3] B. Wang, et al., In search of preventive strategies: novel high-CBD Cannabis sativa extracts modulate ACE2 expression in COVID-19 gateway tissues, Aging (2020) 22425–22440.
[4] M.A. Crocq, History of cannabis and the endocannabinoid system, Dialogues Clin. Neurosci. 22 (3) (2020) 223–228.
[5] K.B. Walsh, A.E. McKinney, A.E. Holmes, Minor cannabinoids: biosynthesis, molecular pharmacology and potential therapeutic uses, in: Frontiers in Pharmacology, 2021, pp. 1–18.
[6] R. Quinones, et al., Quantification of cannabis in infused consumer products and their residues on skin, ACS Pharmacol Transl Sci 5 (8) (2022) 642–651.
[7] L. Cristino, T. Bisogno, V. Di Marzo, Cannabinoids and the expanded endocannabinoid system in neurological disorders, Nat. Rev. Neurol. 16 (1) (2020) 9–29.
[8] O. Devinsky, E. Marsh, D. Friedman, Cannabidiol in patients with treatment-resistant epilepsy - authors' reply, Lancet Neurol. 15 (6) (2016) 545–546.
[9] O. Devinsky, et al., Trial of cannabidiol for drug-resistant seizures in the Dravet syndrome, N. Engl. J. Med. 376 (21) (2017) 2011–2020.
[10] V. Desaulniers Brousseau, et al., Cannabinoids and terpenes: how production of photo-protectants can be manipulated to enhance Cannabis sativa L, Phytochemistry. Front Plant Sci 12 (2021) 620021.

[11] F. Taura, et al., Purification and characterization of cannabidiolic-acid synthase from *Cannabis sativa* L. Biochemical analysis of a novel enzyme that catalyzes the oxidocyclization of cannabigerolic acid to cannabidiolic acid, J. Biol. Chem. (1996) 17411–17416 (Â© 1996 ASBMB. Currently published by Elsevier Inc; originally published by American Society for Biochemistry and Molecular Biology).

[12] S. Sirikantaramas, et al., The gene controlling marijuana psychoactivity. Molecular cloning and heterologous expression of Δ1-tetrahydrocannabinolic acid synthase from *Cannabis sativa* L, J. Biol. Chem. (2004) 39767–39774 (Â© 2004 ASBMB. Currently published by Elsevier Inc; originally published by American Society for Biochemistry and Molecular Biology).

[13] K.J.H. Lim, et al., Biosynthesis of nature-inspired unnatural cannabinoids, in: Molecules, 2021.

[14] C.M. Andre, J.-f. Hausman, G. Guerriero, *Cannabis sativa*: The Plant of the Thousand and One Molecules, 2016, pp. 1–17.

[15] L. Dai, R. Luo, L. Zhang, S. Zhang, Y. Kang, J. Chi, X. Feng, J. Shi, Y. Tian, B. Gao, Z. Li, Improvement of cannabidiolic acid synthetase activity through molecular docking and site-directed mutagenesis, Ind. Crop. Prod. 208 (2024) 117860–117875.

[16] J. de A. Leite, et al., Extraction and isolation of cannabinoids from marijuana seizures and characterization by (1)H NMR allied to chemometric tools, Sci. Justice 58 (5) (2018) 355–365.

[17] T. Ohtsuki, et al., Selective preparation and high dynamic-range analysis of cannabinoids in "CBD oil" and other Cannabis sativa preparations, J. Nat. Prod. (2022) 634–646.

[18] E. Chiurchiù, S. S., P. Allegrini, D. Ciceri, R. Ballini, A. Palmieri, A novel and practical continuous flow chemical synthesis of Cannabidiol (CBD) and its CBDV and CBDB analogues, Eur. J. Org. Chem. 2021 (2021) 1286–1289.

[19] L.J. Kearsey, et al., Structure of the Cannabis sativa olivetol-producing enzyme reveals cyclization plasticity in type III polyketide synthases, FEBS J. (2019) 1–14.

[20] Y. Shoyama, et al., Structure and function of δ 1-tetrahydrocannabinolic acid (THCA) synthase, the enzyme controlling the psychoactivity of *Cannabis sativa*, J. Mol. Biol. (2012) 96–105 (Elsevier Ltd.).

[21] Zirpel, B., F. Stehle, and O. Kayser, Production of delta9-tetrahydrocannabinolic acid from cannabigerolic acid by whole cells of Pichia (Komagataella) pastoris expressing delta9-tetrahydrocannabinolic acid synthase from *Cannabis sativa* L., in Biotechnology Letters. 2015. p. 1869–1875.

[22] B. Zirpel, et al., Engineering yeasts as platform organisms for cannabinoid biosynthesis, in: Journal of Biotechnology, Elsevier, 2017, pp. 204–212.

[23] B. Zirpel, et al., Optimization of Δ9-tetrahydrocannabinolic acid synthase production in Komagataella phaffii via post-translational bottleneck identification, in: Journal of Biotechnology, Elsevier, 2018, pp. 40–47.

[24] X. Luo, et al., Complete biosynthesis of cannabinoids and their unnatural analogues in yeast, in: Nature, Springer US, 2019, pp. 123–126.

[25] T. Gülck, et al., Synthetic biology of cannabinoids and cannabinoid glucosides in Nicotiana benthamiana and Saccharomyces cerevisiae, J. Nat. Prod. (2020) 2877–2893.

[26] Kosalková, K.B., C.; Sánchez-Orejas, I.C.; Cueto, L.; García-Estrada, C., Biotechnological fungal platforms for the production of biosynthetic cannabinoids. Journal of Fungi, 2023.

[27] F. Awwad, et al., Bioengineering of the marine diatom Phaeodactylum tricornutum with cannabis genes enables the production of the cannabinoid precursor, olivetolic acid, Int. J. Mol. Sci. 24 (23) (2023).

[28] Fantino, E.A., F.; Merindol, N.; Diaz Garza, A.M.; Gelinas, S.E; Gajon Robles, G.C.; Custeau, A.; Meddeb-Mouelhi, F.; Desgagne-Penix, I., Bioengineering Phaeodactylum tricornutum, a marine diatom, for cannabinoid biosynthesis. Algal Res., 2024.

[29] K. Blatt-janmaat, Y. Qu, The Biochemistry of Phytocannabinoids and Metabolic Engineering of Their Production in Heterologous Systems, 2021.

[30] S. Sirikantaramas, et al., Tetrahydrocannabinolic Acid Synthase, the Enzyme Controlling Marijuana Psychoactivity, is Secreted Into the Storage Cavity of the Glandular Trichomes, 2005, pp. 1578–1582.

[31] M. Geissler, et al., Subcellular localization defines modification and production of D9-tetrahydrocannabinolic acid synthase in transiently transformed Nicotiana benthamiana, in: Biotechnology Letters, Springer Netherlands, 2018, pp. 913–919.

[32] Schmidt, C.A., M.; Kayser, O., Engineering cannabinoid production in Saccharomyces cerevisiae. Biotechnol. J., 2024.

[33] Hu, J.M., W.; Su, Y.; Qian, C.; Fu, W., Emerging technologies for advancing microalgal photosynthesis and metabolism toward sustainable production. Frontiers, 2023.

[34] A. Einhaus, T. Baier, O. Kruse, Molecular design of microalgae as sustainable cell factories, Trends Biotechnol. 42 (6) (2024) 728–738.

[35] D. Sethi, et al., Diatoms for carbon sequestration and bio-based manufacturing, Biology (Basel) 9 (8) (2020).

[36] D. Ova Ozcan, B. Ovez, Evaluation of the interaction of temperature and light intensity on the growth of Phaeodactylum tricornutum: kinetic modeling and optimization, Biochem. Eng. J. 154 (2020) 107456 (Elsevier).

[37] Cui, Y.T.-H., S.R.; Chua, E.T.; Schenk, P.M., Development of high-level omega-3 eicosapentaenoic acid (EPA) production from Phaeodactylum tricornutum. J. Phycol., 2021.

[38] A.C. Jaramillo-Madrid, et al., Overexpression of key sterol pathway enzymes in two model marine diatoms alters sterol profiles in *phaeodactylum tricornutum*, in: Pharmaceuticals, 2020, pp. 1–19.

[39] M. Fabris, et al., Extrachromosomal genetic engineering of the marine diatom *Phaeodactylum tricornutum* enables the heterologous production of monoterpenoids, in: ACS Synthetic Biology, 2020, pp. 598–612.

[40] J. George, et al., Metabolic engineering strategies in diatoms reveal unique phenotypes and genetic configurations with implications for algal genetics and synthetic biology, in: Frontiers in Bioengineering and Biotechnology, 2020, pp. 1–19.

[41] E. Erdene-ochir, et al., Identification and characterisation of the novel endogenous promoter HASP1 and its signal peptide from Phaeodactylum tricornutum, in: Scientific Reports, Springer US, 2019, pp. 1–10.

[42] S.S. Slattery, et al., Phosphate - regulated expression of the SARS - CoV - 2 receptor - binding domain in the diatom Phaeodactylum tricornutum for pandemic diagnostics, in: Scientific Reports, Nature Publishing Group UK, 2022, pp. 1–15.

[43] R.J. Jenny, K.G. Mann, R.L. Lundblad, A critical review of the methods for cleavage of fusion proteins with thrombin and factor Xa, Protein Expr. Purif. 31 (1) (2003) 1–11.

[44] BioRender, BioRender. 2023.

[45] K.E. Apt, et al., In vivo characterization of diatom multipartite plastid targeting signals, J. Cell Sci. 115 (Pt 21) (2002) 4061–4069.

[46] O. Kilian, P.G. Kroth, Identification and characterization of a new conserved motif within the presequence of proteins targeted into complex diatom plastids, in: The Plant Journal: For Cell and Molecular Biology, 2005, pp. 175–183.

[47] X. Liu, et al., Addressing various compartments of the diatom model organism *Phaeodactylum tricornutum* via sub-cellular marker proteins, in: Algal Research, Elsevier B.V., 2016, pp. 249–257.

[48] N. Lingg, et al., The sweet tooth of biopharmaceuticals: importance of recombinant protein glycosylation analysis, Biotechnol. J. 7 (12) (2012) 1462–1472.

[49] E. Erdene-Ochir, et al., Cloning of a novel endogenous promoter for foreign gene expression in Phaeodactylum tricornutum, in: Applied Biological Chemistry, Springer Netherlands, 2016, pp. 861–867.

[50] S. Sosa-Carrillo, et al., Maximizing protein production by keeping cells at optimal secretory stress levels using real-time control approaches, Nat. Commun. 14 (1) (2023) 3028.

[51] A. Messaabi, et al., In vivo thrombin activity in the diatom Phaeodactylum tricornutum: biotechnological insights, Appl. Microbiol. Biotechnol. 108 (1) (2024) 481.

[52] A. Diamond, et al., Instability of Extrachromosomal DNA Transformed Into the Diatom *Phaeodactylum tricornutum*, 2023.

[53] B. Zirpel, O. Kayser, F. Stehle, Elucidation of structure-function relationship of THCA and CBDA synthase from Cannabis sativa L, in: Journal of Biotechnology, Elsevier, 2018, pp. 17–26.

[54] Cox, J.S.W., P., A Novel Mechanism for Regulating Activity of a Transcription Factor That Controls the Unfolded Protein Response. 1996.

[55] Slattery, S.S., et al., An expanded plasmid-based genetic toolbox enables Cas9 genome editing and stable maintenance of synthetic pathways in *Phaeodactylum tricornutum.*, in ACS Synthetic Biology. 2018. p. 328–338.

[56] B.J. Karas, et al., Designer diatom episomes delivered by bacterial conjugation, in: Nature Communications, Nature Publishing Group, 2015, pp. 1–10.

[57] M.A. Valliere, et al., A cell-free platform for the prenylation of natural products and application to cannabinoid production, in: Nature Communications, Springer US, 2019, pp. 1–9.

[58] N. Sharma, et al., Impact of different light characteristics on the growth and lipid content of diatom Phaeodactylum tricornutum transconjugant strains, Am. J. Plant Sci. (2023) 41–63.